Asia-Pacific J. Atmos. Sci., 47(2), 167-180, 2011
DOI:10.1007/s13143-011-0006-y

Sensitivity of the WRF Model Simulation of the East Asian Summer Monsoon in 1993 to Shortwave Radiation Schemes and Ozone Absorption

Hyung-Jin Kim[1] and Bin Wang[2]

[1]*Research Institute for Global Change, Japan Agency for Marine-Earth Science and Technology, Kanazawa-ku, Yokohama, Japan*
[2]*International Pacific Research Center and Department of Meteorology, School of Ocean and Earth Science and Technology, University of Hawaii at Manoa, Hawaii, U.S.A.*

(Manuscript received 5 April 2010; revised 17 November 2010; accepted 21 November 2010)

Abstract: Sensitivity of the Weather Research and Forecasting (WRF) model simulation of the East Asian summer monsoon (EASM) in 1993 to solar radiation parameterizations and ozone absorption was investigated. Three numerical experiments were conducted using the National Centers for Environmental Prediction/Department of Energy (NCEP/DOE) and the European Centre for Medium-Range Weather Forecasts (ECMWF) reanalysis data as time-varying surface and lateral boundary forcings, respectively: (a) a control run ("CTL") with the Dudhia radiation scheme and the model top placed at 50 hPa, (b) the "SWG" experiment which is the same as the CTL except the Goddard radiation scheme, and (3) the "SWT" run which is the same as the SWG but the model top was raised to 5 hPa and the vertical levels increased from 31 to 35. The use of the Goddard scheme results in considerable improvement in reproducing the model's thermal structures, such as zonal mean air temperature, its latitudinal gradient and vertically integrated temperature. This leads to better agreements in the simulation of the upper tropospheric zonal winds through the thermal wind relationship which, in turn, rectifies the low-level circulations through dynamical coupling between the upper and lower troposphere. The Taylor diagram analysis quantitatively indicates that the SWT and the SWG are discernable from each other with slightly improved simulations in the SWT. This suggests a nontrivial role of ozone absorption and accompanied stratospheric heating in EASM simulation.

Key words: East Asian summer monsoon, WRF model, shortwave radiation, maximum ozone height, ozone absorption, model-top layer

1. Introduction

Changes in the intensity and location of the upper-level westerly jet significantly affect the activity and displacement of the subtropical front known as Meiyu (China), Changma (Korea) or Baiu (Japan). During the summer of 1994, for example, the severe drought was prevailed over central China, South Korea and southern Japan in association with the northward shift of the suppressed jet (Park and Schubert, 1997; Lee and Suh 2000; Lee *et al.,* 2002). Meanwhile the southward migration of the enhanced 200-hPa westerly winds was concurrent with serious summer-time flooding in 1991, 1993 and 1998 over the aforementioned regions (Lee and Suh, 2000; Wang *et al.,* 2000; Lee *et al.,* 2004; Yoo *et al.,* 2004; Kang *et al.,* 2005). The anomalous water vapor transport associated with the southward shift of the upper level jet is deemed essential for the abundant precipitation (Zhou and Yu, 2005). The upper air confluence also more often modulates frontal activity through inducing secondary circulations that favor instability on the right (left) side of the jet entrance (exit) (Blackmon *et al.,* 1977). At the surface, a large-scale low formed over the Asia continent drives low-level monsoon flows which regulate the moisture transport from the South China Sea to East Asia and largely control the monsoon rainfall amount in an interactive sense (Ding 1992; Kawamura and Murakami, 1998).

Of note is that both upper- and low-level circulations are closely related to large-scale temperature structures. The upper air jet is a balanced response to the northward temperature gradient (Zhang *et al*., 2006) and the low-level monsoon flows are accentuated by the differential heating between the Asia continent and the adjacent oceans. From the numerical modeling viewpoint, therefore, the realistic simulation of the large-scale temperature is imperative to better represent the intensity and displacement of the East Asia summer monsoon (EASM).

Numerical model consists of various physical parameterizations. Among others, careful consideration should be placed on the radiation processes for the simulation on timescales from subseasonal to annual because in these timescales radiative heating rate could be significant compared to advective and condensational heating rate (Giorgi and Mearns, 1999). In the present study, the authors investigate the sensitivity of the simulated regional summer climate to solar radiation parameterizations by utilizing regional climate model (RCM) simulations. Also examined are the effects of the model's top and stratospheric vertical resolution that determines ozone absorption of shortwave radiation. The observed ozone profile generally shows a maximum between 10 hPa and 5 hPa (Fortuin and Kelder, 1998). In a large body of previous RCM studies, however, the upper boundary was set at a level much lower than the ozone maximum height.

To test model sensitivity, the EASM in 1993 was simulated and validated against observation as rainfall and atmospheric circulations in this particular summer were deviated from their climatology over the large parts of East Asia (Lee and Suh,

Corresponding Author: Hyung-Jin Kim, Research Institute for Global Change, Japan Agency for Marine-Earth Science and Technology, 3173-25 Showa-machi, Kanazawa-ku, Yokohama, Kanagawa 236-0001, Japan.
E-mail : hyungjin@jamstec.go.jp

2000; Yoo *et al.,* 2004). The regional model used is the Weather Research and Forecasting (WRF) model that has recently taken the priority of regional model development from many institutes, centers, and universities. Though the WRF is primarily aimed to short-term prediction, the use of it in regional climate study has been rapidly increased in recent years (Davis *et al.,* 2003; Knievel *et al.,* 2004; Lo *et al.,* 2008; Salathé *et al.,* 2010).

This paper is organized as follows. Section 2 presents the observed characteristics of the anomalous summer monsoon in 1993. Model description and design of sensitivity tests are presented in section 3. Sensitivity to solar radiation schemes and top boundary layers is illustrated and discussed in section 4. The last section gives summary with concluding remarks.

2. East Asian summer monsoon in 1993

The observed features of the atmospheric circulation and precipitation were briefly documented by using the ECMWF 40-year reanalysis (ERA, Uppala *et al.,* 2005) and the Chinese station data merged with the Global Precipitation Climatology Project (GPCP) version 2 data (Alder *et al.,* 2003). The station precipitation was recorded at about 700 meteorological stations across China and archived by the Climate Data Center of National Meteorological Information Center, China Meteorological Administration. To construct anomalies, a 20-year average over 1981-2000 was used as a climatology.

a. Zonal mean air temperature and westerly jet

Figure 1 shows the observed June-July-August (JJA) zonal mean air temperature and its anomaly. The air temperature decreases upward and poleward in the mid-latitude troposphere, whereas above 100 hPa opposite tendency is seen owing to the existence of the upper-level cold core. The anomaly patterns display colder (warmer)-than-normal temperature in middle latitude troposphere (stratosphere), implying an intensification of meridional temperature gradient.

Figure 2 represents latitude-height cross sections of the northward temperature gradient (shadings) and zonal winds (contours) for the climatological JJA mean (Fig. 2a), the 1993 JJA mean (Fig. 2b), and the anomalous zonal winds in 1993 (Fig. 2c). The temperature gradient was estimated by $-\Delta\overline{T}/(\Delta\phi) = -(\overline{T}_{j+1}-\overline{T}_j)/\Delta\phi$ ($\Delta\phi$ is 2.5° and j is a latitudinal index) so that positive (negative) temperature gradient denotes westerly (easterly) shear. The axis of the climatological jet is located at 200 hPa around 40°N with maximum speed of about 25 m s^{-1}. In 1993, the upper-level westerly jet is intensified by about 5 m s^{-1} in association with the enhanced tropospheric temperature gradient (Fig. 2b). The thermal wind relationship is robust in that the height where the meridional temperature gradient vanishes (the thick lines in Figs. 2a and 2b) coincides well with the maximum westerly winds height. Also evident is the slight southward displacement of jet streak, resulting in positive anomalies in the extra-tropics and negative anomalies to the north and the south (Fig. 2c).

Shown in the left and right panels of Fig. 3 are the monthly anomaly of 850-hPa relative vorticity superimposed with the 200-hPa zonal winds and precipitation anomaly, representing the upper- and low-level dynamical linkage and the impacts of low-level circulation on precipitation, respectively. In June 1993, little evidences are found for the dynamical coupling between the upper- and low-level anomalous circulations (Fig. 3a). During the rest two months, on the other hand, positive vorticity anomaly occurs in a narrow band of intensified westerly jet located mostly over the southern Korea and Japan (Figs. 3b and 3c). It is also seen that the cyclonic vorticity anomaly coexists with the increased rainfall over Korea and Japan (Figs. 3e and 3f). Thus, the intensified westerly winds aloft tend to induce positive vorticity anomaly which results in the increased precipitation. Another interesting feature is that the above-normal rainfall in June and July over southern China seems to have nothing to do with 850-hPa vorticity anomaly, implying that the "rain-enhancing" mechanism over south China is likely different from that over Korea and Japan.

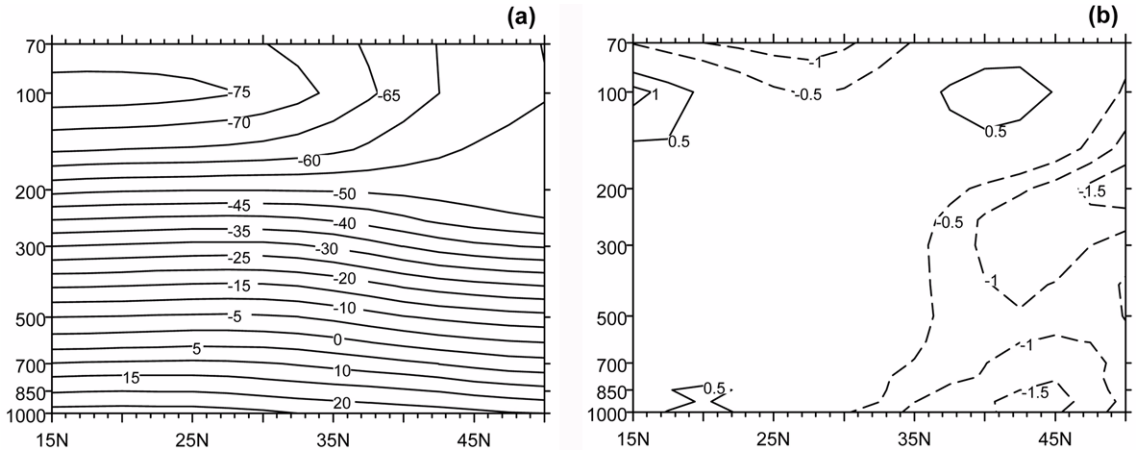

Fig. 1. Latitude-height cross section of (a) the JJA air temperature in 1993 and (b) its anomaly obtained from the ECMWF 40-year reanalysis. Units are in °C.

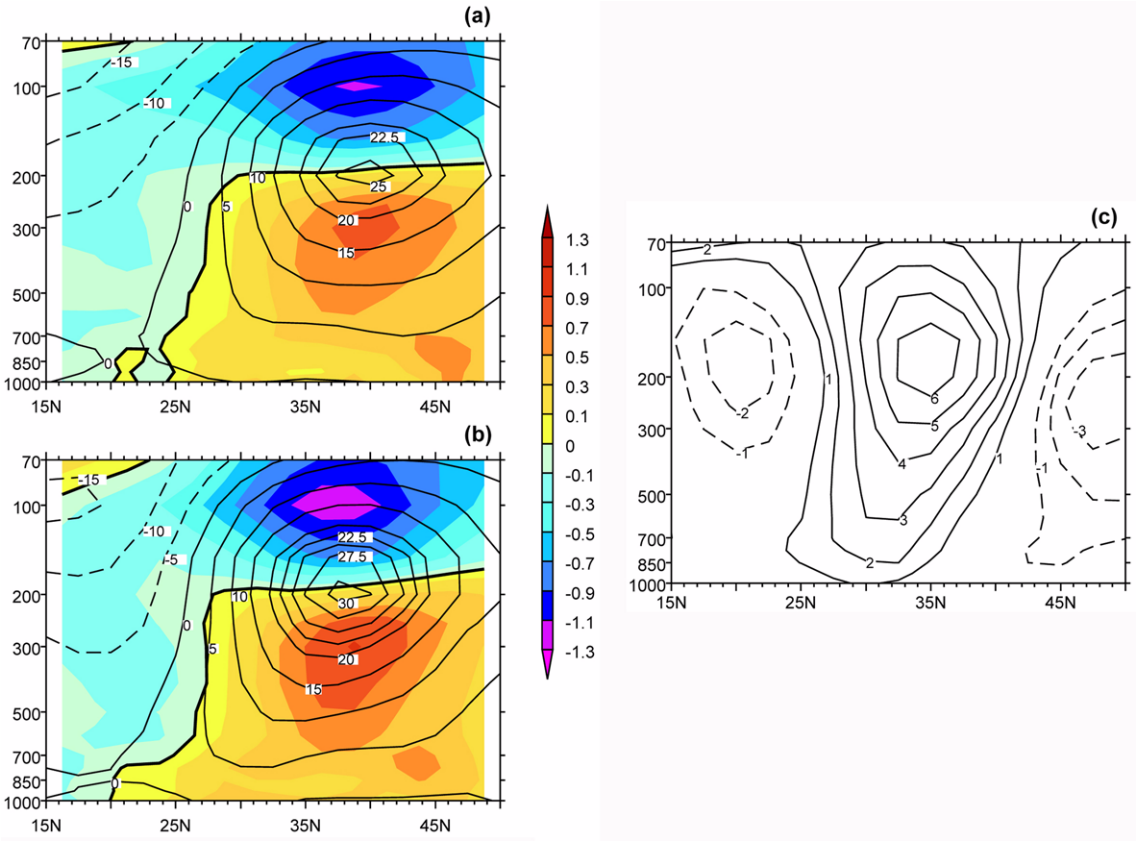

Fig. 2. Latitude-height cross section of the JJA zonal winds (contours, m s^{-1}) and latitudinal temperature gradient (shadings, °C/deg-lat) (a) for 20-year climatology and (b) in 1993. (c) is for the zonal winds anomaly (m s^{-1}) in 1993. In (a) and (b), contour intervals are 5 within ± 20 and 2.5 outside, and positive (negative) temperature gradient denotes westerly (easterly) shear. Thick solid line in (a) and (b) indicates zero temperature gradient.

b. Atmospheric heat source and monsoon circulations

The Asian summer monsoon circulations characterized by upper air northeasterly and low-level southwesterly are closely related to the atmospheric heat source induced by a differential heating between land and ocean. The spatial patterns and temporal evolution of the monsoon flows can be traced by the middle tropospheric temperature (Ueda and Yasunari, 1998; He *et al.,* 2003; Goswami and Xavier, 2005). In this respect, the vertically integrated temperature between 600 and 200 hPa (VIT hereinafter) was examined by using the ERA to reveal the anomalous features of the atmospheric thermal structure and associated monsoon circulations.

Figure 4a represents the JJA VIT in 1993 over the Asian monsoon regions. The shaded areas delineate the warm core with temperature warmer than −16°C, while the thick lines denote the locations where the direction of the 200-hPa zonal winds changes (in other words, the ridge of the South Asian high). The major heat sources are resided on the South Asian continent and the upper-level ridge is aligned with the local temperature maxima. Figure 4b shows the VIT anomaly (shadings) and 200-hPa wind anomaly (vectors). The VIT anomaly warmer than 0.1°C is found only in the southeastern parts of China and accompanied with the enhanced anticyclone. The anomalous heat source also results in an intensified heat low and leads to the increased low-level southerly on the southeast coast of China (Fig. 4c), providing an enhanced moisture transport. This could be responsible for the larger-than-normal precipitation over southeastern China mentioned previously in section 2a.

3. Model description and numerical experiments

a. The WRF model

The WRF model is developed for both research purpose and operational prediction of mesoscale atmospheric phenomena with the horizontal grid scale from several to hundreds km. The WRF model consists of a fully compressible, three-dimensional, nonhydrostatic core formulated using terrain-following mass vertical coordinate (Skamarock *et al.,* 2005). The governing equations are written in a flux form. The Runge-Kutta schemes and high-order advection schemes are adopted for numerical integration of prognostic equations (Wicker and Skamarock, 2002).

The Monin-Obukhov surface-layer scheme (Dyer and Hicks, 1970; Paulson, 1970; Webb, 1970), the Noah land surface model (Chen and Dudhia, 2001), and the Yonsei University (YSU) boundary-layer parameterization (Hong *et al.,* 2006) are selected

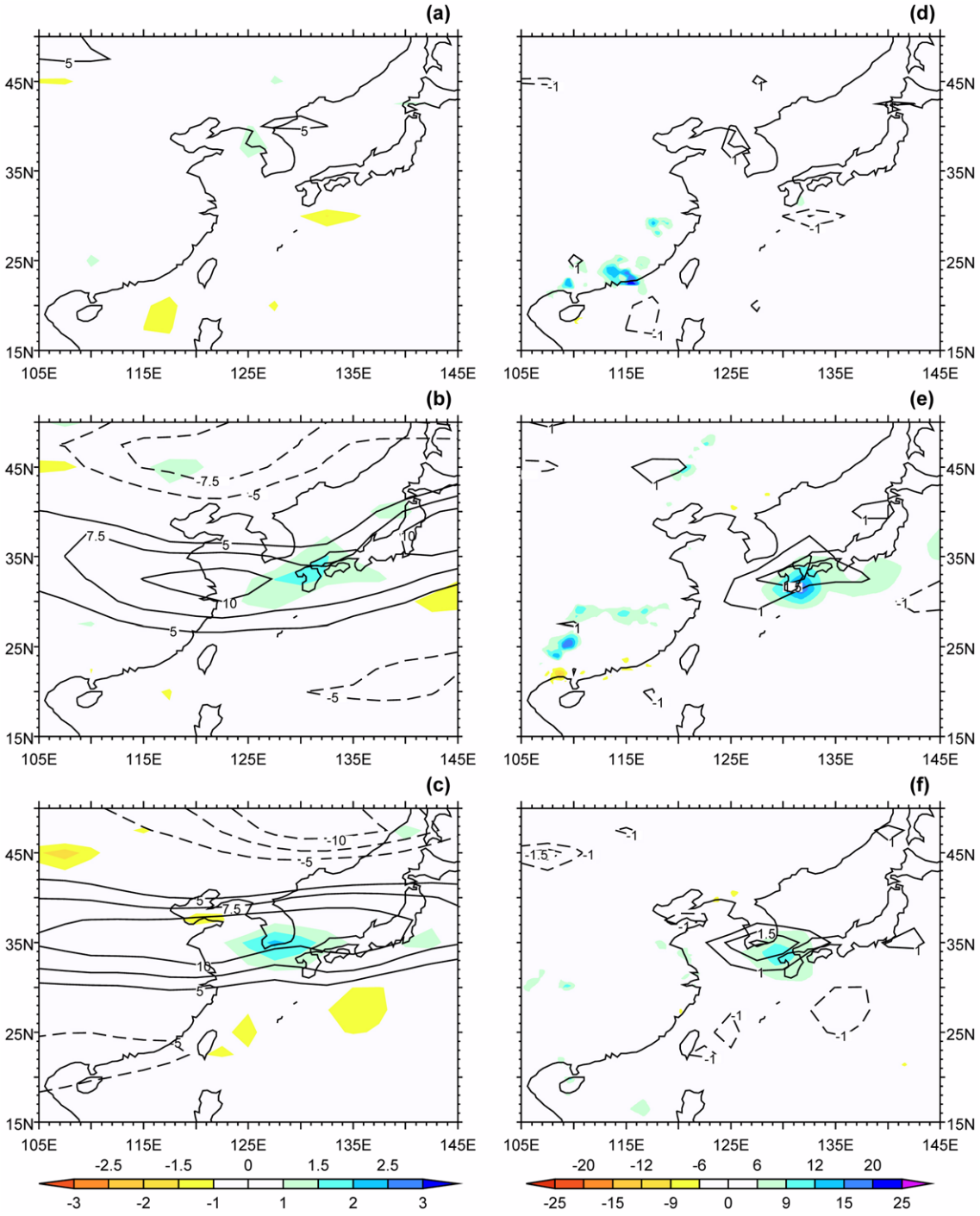

Fig. 3. The observed anomaly of 850-hPa relative vorticity (10^5 s^{-1}, shadings in left and contours in right) with (left) 200-hPa zonal winds (contours, m s^{-1}) and (right) precipitation (shadings, mm d^{-1}). (a, d), (b, e) and (c, f) are for June, July and August in 1993, respectively. Contour intervals are ± 5, ± 7.5 and ± 10 for zonal winds and ± 1, ± 1.5 and ± 2 for relative vorticity, respectively.

from the various built-in packages to represent near surface processes. The Betts-Miller-Janjić scheme (Janjić, 1994) and the Lin Microphysics scheme (derived from the original scheme described in Lin *et al.*,, 1983) are chosen for convective and microphysical processes, respectively. Terrestrial radiation is parameterized by the rapid radiative transfer model (Mlawer *et al.,* 1997; Iacono *et al.,* 2000). Table 1 gives a brief description of the numerical configurations and the selected parameterizations.

b. Numerical experiments

The model domain consists of 145 by 115 grid points in the zonal and meridional directions, respectively, with a grid resolution of 50 km centering at 35°N and 120°E (Fig. 5). It covers the

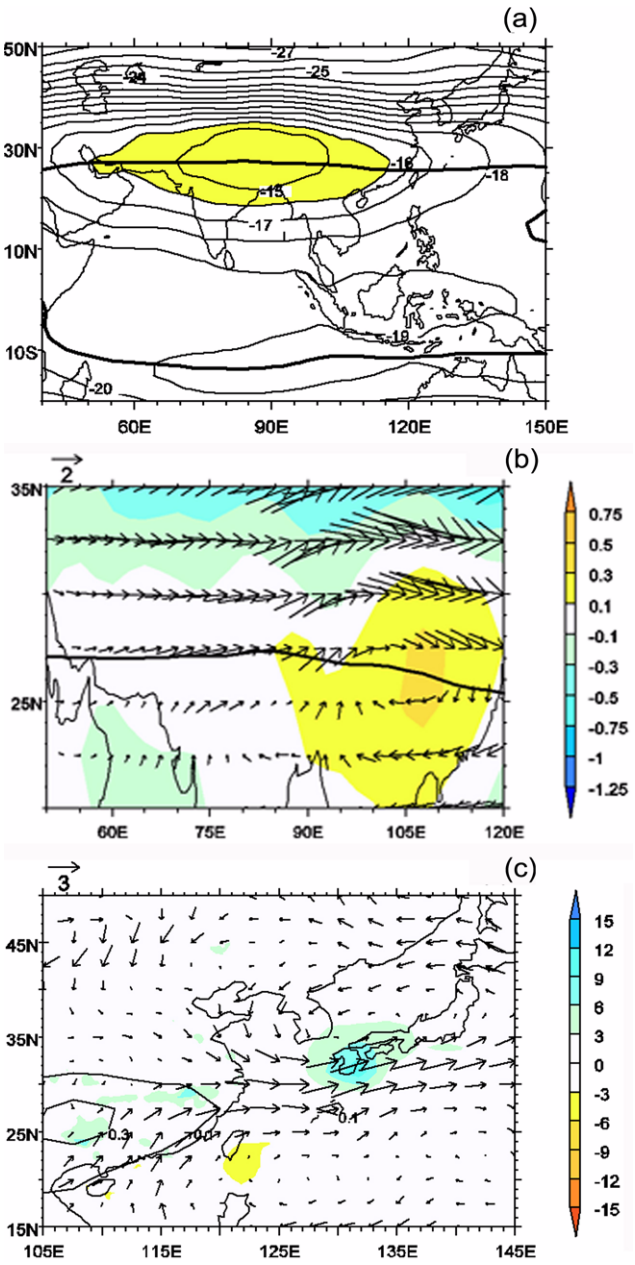

Fig. 4. (a) The observed JJA mean VIT (°C) over the Asian monsoon regions in 1993 with shadings for the regions warmer than −16°C. (b) VIT (shadings, °C) and 200-hPa wind (vectors, m s^{-1}) anomaly in 1993. (c) 850-hPa wind (vectors, m s^{-1}) and precipitation (shadings, mm d^{-1}) anomaly in 1993. In (a) and (b) thick solid lines indicate zero lines of 200-hPa zonal winds.

majority of the East Asia continent, including most part of the Tibetan Plateau and the Indochina Peninsula. Also included are a part of Bay of Bengal, the South China Sea and the western Pacific Ocean where the differential heating between land and adjacent ocean is prominent (He *et al.,* 2003). Thus, the domain is large enough to consider the land-sea thermal contrast and modulation of upper air flows due to high topography.

The selected grid distance of 50 km is in the range of the suggested ratio of 3-8 between driving data and model resolution (Giorgi and Mearns, 1999) because the NCEP/DOE reanalysis (NRA2, Kanamitsu *et al.,* 2002) for surface boundary condition and the ERA for lateral boundary condition has the resolution of $1.875^{\circ} \times \sim 2^{\circ}$ and $2.5^{\circ} \times 2.5^{\circ}$, respectively. The model simulations with the integration time step of $\Delta t = 180$ s are initialized on 1 May 1993 and performed to 31 August 1993 with lateral boundary data updated every 6 hours. Time-varying sea surface temperatures are also prescribed for water surface with the same interval.

Three numerical experiments were carried out to test model's sensitivity to the shortwave radiation schemes and shortwave absorption of ozone. First, a control run ("CTL") was conducted with the simple shortwave radiation scheme (Dudhia, 1989) with the top boundary placed at 50 hPa. Second, the "SWG" experiment was performed in which the Goddard shortwave scheme (Chou and Suarez, 1999) was employed with the same vertical configuration as the CTL. The last numerical integration ("SWT") also utilized the Goddard shortwave scheme but with the upper boundary at 5 hPa. The number of total vertical levels is 31 for the first two simulations and 35 for the last. Each simulation has one "effective layer" that extends from the prescribed model top to about 0.0006 hPa to calculate incident

Table 1. Numerical configurations and physics parameterizations for the numerical experiments.

Features	Selected value/option
Integration time step	180 s
Horizontal resolution	50 km
Integration period	1 May 1993 - 31 August 1993
Analysis period	1 June 1993 - 31 August 1993
Surface B. C.	Reanalysis-2 (6-hour interval)
Lateral B. C.	ERA (6-hour interval)
Cumulus convection	Betts-Miller-Janjić (cudt = 30 min)
Cloud microphysics	Lin
Surface layer	Monin-Obukhov
PBL	YSU (bldt = 180 s)
Land surface	Noah
Longwave radiation	RRTM (radt = 30 min)
Solar constant	1365 W m^{-2}

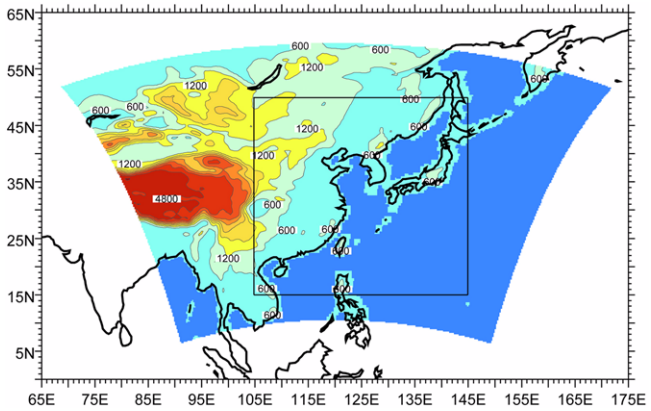

Fig. 5. Model domain and topographic height (m) with a grid spacing of 50 km. Contour interval is 600 m. The boxed region denotes the analysis domain.

shortwave flux reaching at the model's top layer. If the surface pressure in the WRF model varies from 1000 hPa to 900 hPa, the SWT would have additional 7 levels between 50 hPa and 5 hPa (see Table 3). Note that the number of levels in PBL (below 850 hPa) is not significantly different between the 50-hPa and 5-hPa experiments. A summary of the numerical experiments and the vertical levels are given in Table 2 and 3, respectively.

The shortwave parameterization of Dudhia (1989) (Dudhia scheme, hereafter) has no spectral bands and, thus, is not able to reflect the rapidly varying shortwave flux with wavenumber. Further simplification is the implicit treatment of the absorption of ozone and minor gases such as O_2 and CO_2. In contrast, shortwave fluxes in Chou and Suarez (1999) (Goddard scheme, hereafter) are integrated from 0.175 to 10 μm which are divided further into eleven sub-bands. Especially, attenuation of ozone that is important in determining the stratospheric temperature is explicitly calculated in the ultraviolet and visible regions.

Table 2. Design of the numerical experiments.

	CTL	SWG	SWT
Shortwave radiation	Dudhia	Goddard	Goddard
Top boundary	50 hPa	50 hPa	5 hPa
Vertical levels	31	31	35

Table 3. The prescribed vertical σ (pressure normalized by surface pressure) levels and corresponding pressures used in the CTL, the SWG and the SWT experiment. Here, the pressure levels are obtained using the given top boundary in Table 2 and the assumed surface pressures of 1000 hPa and 900 hPa. Shaded values indicate additional pressure levels in 50 hPa to 5 hPa used in the SWT.

Level index	CTL and SWG			SWT		
	σ	pressure (p_s = 1000)	pressure (p_s = 900)	σ	pressure (p_s = 1000)	pressure (p_s = 900)
1	1.000	1000.0	900.0	1.000	1000.0	900.0
2	0.993	993.4	894.0	0.993	993.0	893.7
3	0.980	981.0	883.0	0.980	980.1	882.1
4	0.966	967.7	871.1	0.966	966.2	869.6
5	0.950	952.5	857.5	0.950	950.3	855.3
6	0.933	936.4	843.1	0.933	933.3	840.0
7	0.913	917.3	826.0	0.913	913.4	822.1
8	0.892	897.4	808.2	0.892	892.5	803.3
9	0.869	875.5	788.7	0.869	869.7	782.8
10	0.844	851.8	767.4	0.844	844.8	760.4
11	0.816	825.2	743.6	0.816	816.9	735.3
12	0.786	796.7	718.1	0.786	787.1	708.5
13	0.753	765.4	690.0	0.753	754.2	678.9
14	0.718	732.1	660.3	0.718	719.4	647.6
15	0.680	696.0	628.0	0.680	681.6	613.6
16	0.639	657.0	593.2	0.639	640.8	576.9
17	0.596	616.2	556.6	0.596	598.0	538.4
18	0.550	572.5	517.5	0.550	552.3	497.3
19	0.501	525.9	475.8	0.501	503.5	453.4
20	0.451	478.5	433.4	0.451	453.7	408.6
21	0.398	428.1	388.3	0.398	401.0	361.2
22	0.345	377.8	343.3	0.345	348.3	313.8
23	0.290	325.5	296.5	0.290	293.5	264.5
24	0.236	274.2	250.6	0.236	239.8	216.2
25	0.188	228.6	209.8	0.188	192.1	173.3
26	0.145	187.8	173.3	0.145	149.3	134.8
27	0.108	152.6	141.8	0.108	112.5	101.7
28	0.075	121.3	113.8	0.064	68.7	62.3
29				0.042	46.8	42.6
30				0.028	32.9	30.1
31	0.046	93.7	89.1	0.017	21.9	20.2
32	0.021	69.9	67.8	0.010	14.9	13.9
33	0.000	50.0	50.0	0.006	11.0	10.4
34				0.002	7.0	6.8
35				0.000	5.0	5.0

4. Results

The model simulations except for the precipitation were regridded onto ERA's grid system of $2.5^o \times 2.5^o$ for validation. For the precipitation, finer resolution ($0.5^o \times 0.5^o$) was used thanks to a dense observational network of China station data set.

a. Zonal mean structures

Figure 6 shows latitude-height cross section of the JJA mean air temperature and its bias for the CTL (Figs. 6a and 6d), the SWG (Figs. 6b and 6e) and the SWT (Figs. 6c and 6f), respectively. In these figures, air temperature below 850 hPa is excluded owing to the missing values of the model solution over the high topography. Common errors include moderate negative biases in the troposphere (about -1^oC) and relatively large warm biases in the upper atmosphere (3-5^{o}C). Salient differences, however, exist in the simulation of the upper-level cold core. In the CTL, the temperature inversion observed in the extra-tropical lower stratosphere is absent (Fig. 6a). In contrast, it is reproduced better in the simulations with the Goddard scheme, and in particular in the SWT (Figs. 6b and 6c).

The improved temperature inversion in the SWG and SWT is most likely due to the advanced radiation parameterizations, and hence readily understandable. But why does the SWT outperform the SWG? The stratospheric temperature is mainly controlled by the longwave cooling due to ozone and carbon dioxide and the solar heating by ozone (Liou 2002). The longwave cooling is generally similar in all simulations regardless of the specified top layer since the cooling profiles of carbon dioxide and ozone change little from 50 hPa up to 5 hPa (Fu and Liou, 1992). Unlike the longwave cooling rate, however, the ozone solar heating varies greatly from several degrees per day at 50 hPa to an order of ten degrees per day at 5 hPa (Chou and Suarez, 1999; Liou, 2002). Therefore, it can be inferred that the upper air temperature inversion reproduced better in the SWT than in the SWG is the result of the realistic ozone absorption and associated heating rate due to the extended layers.

Then the next question is how does the extended vertical boundary give rise to the warmer stratospheric temperature in the SWT? It should be first mentioned that the absorbed solar radiation fluxes above 50 hPa may not be substantially different between the SWG and the SWT since the SWG also takes into account ozone shortwave absorption in the "effective layer" based on the mass-weighted ozone concentration (recall the

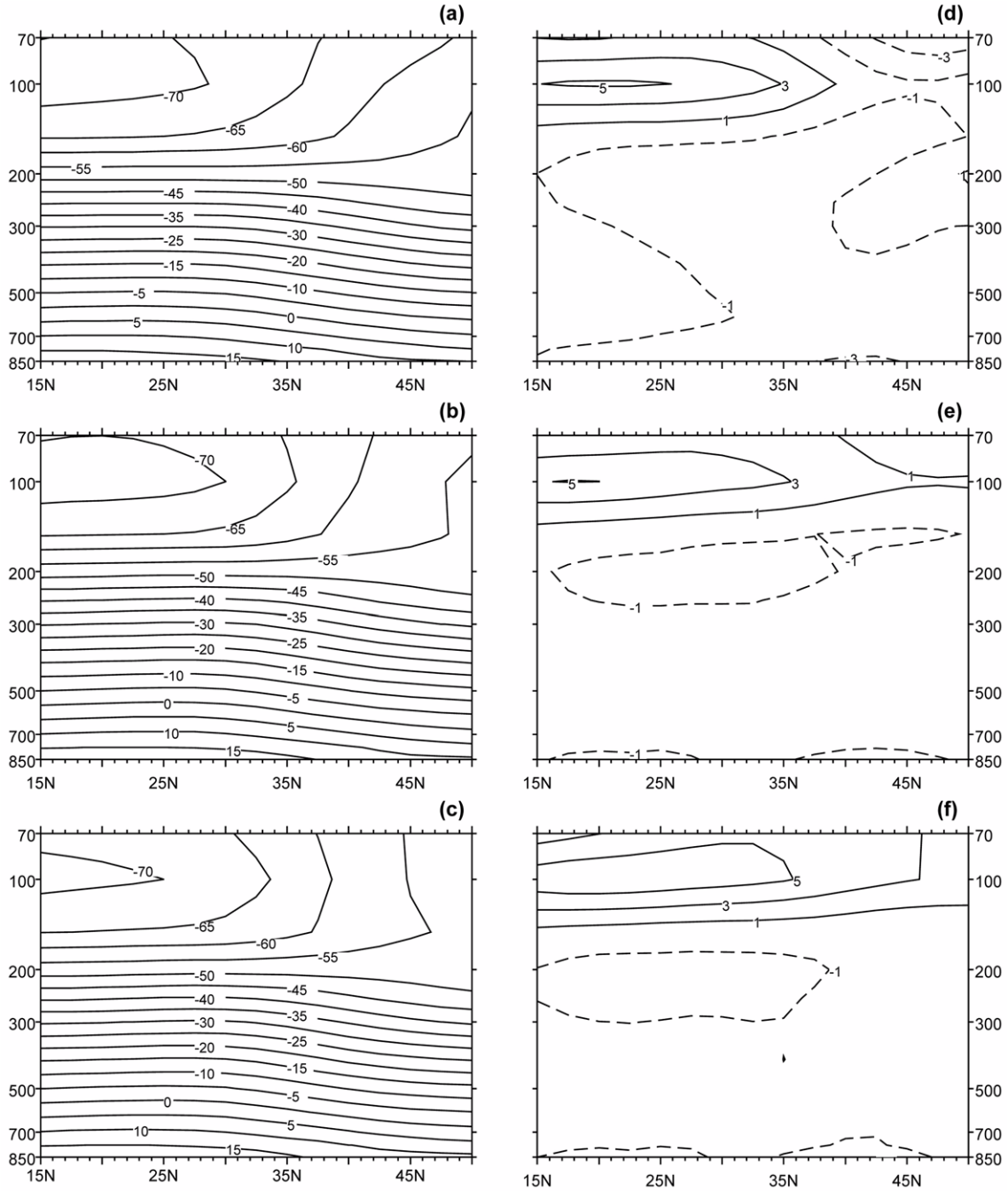

Fig. 6. Latitude-height cross section of the JJA mean air temperature in 1993 (left panels) and its bias (right panels) for (a, d) the CTL, (b, e) the SWG and (c, f) the SWT. Units are in °C.

definition of "effective layer" in section 3b). In fact, further analysis indicates a slight increase of the surface incoming shortwave flux in the SWT (figure not shown), suggesting that the attenuation by ozone is likely reduced in the SWT compared to the SWG. We speculate that the increased number of vertical layers above 50 hPa and the dependency of ozone heating rate on air density are responsible for the improved simulation in the SWT. Air density exponentially decreases in altitude and heating rate is inversely proportional to it. Therefore, heating rate in the lower stratosphere would be very sensitive to the small variation of air density. The SWT has additional 7 layers above 50 hPa (see Table 3), thereby, for the heating rate calculation, it is able to reproduce a more detailed density profile than the SWG which has only one representative value above 50 hPa. As a consequence, the SWT simulates better the ozone heating rate and air temperature in the upper troposphere.

The modeled latitudinal temperature gradient, balanced winds and its anomaly are presented in Fig. 7. The WRF model repro-

duces reasonably well the theoretical thermal-wind relationship: the zero line of the temperature gradients is located at the maximum westerly winds. In the CTL, however, the intensity of the temperature gradients and associated zonal winds are weaker than observed and the three-cell structure in zonal wind anomaly is not properly simulated (Figs. 7a and 7d). These deficits are obviously relieved in the SWG and SWT simulations in which the intensity of the temperature gradient and zonal winds are comparable to the observation (Figs. 7b and 7c) and the spatial patterns of the zonal wind anomaly are adequately organized (Figs. 7e and 7f).

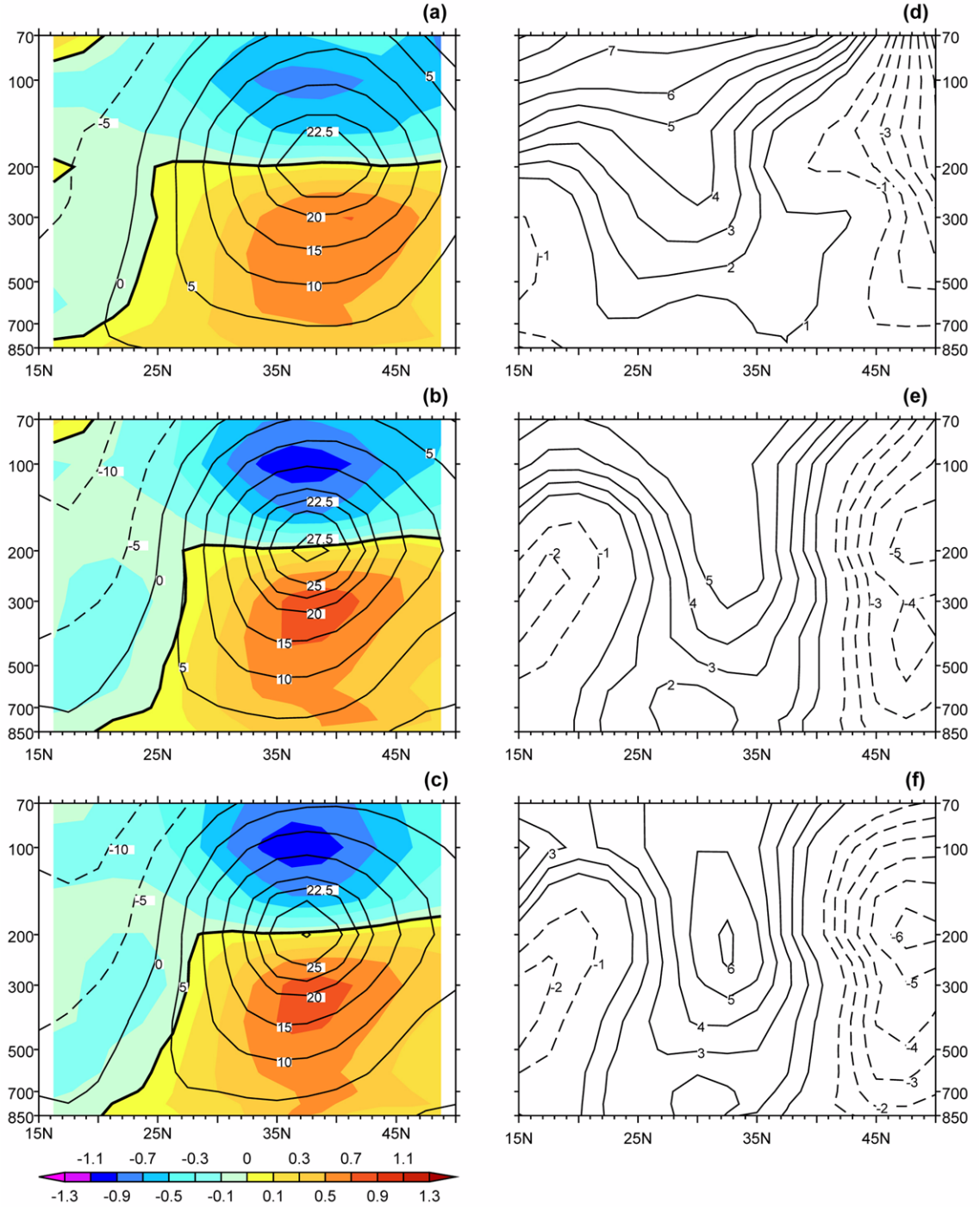

Fig. 7. (Left) Latitude-height cross section of the JJA mean of zonal winds (contours, m s^{-1}) and meridional temperature gradient (shadings, °C/deg-lat) in 1993. Contour intervals are 5 within ± 20 and 2.5 outside, and positive (negative) temperature gradient denotes westerly (easterly) shear. Thick solid line is for zero temperature gradient. (Right) Latitude-height cross section of the JJA zonal winds anomaly (m s^{-1}). Top, middle and bottom panels are for the CTL, the SWG and the SWT, respectively.

b. Linkage between upper- and low-level circulations

Due to the substantial changes in the modeled air temperatures among the three experiments, the upper air flows (for example, 200-hPa zonal winds) also exhibit noticeable alteration and so do the low-level circulations through dynamical coupling. Figure 8 displays the observed and simulated JJA mean 200-hPa zonal winds and 850-hPa vorticity in the summer of 1993. In the observations (Fig. 8a), jet cores are located at 37-40°N with maximum intensities of 30-34 m s^{-1}. When compared to the climatology (figure not shown), they migrates southward and are intensified by about 5 m s^{-1}. Jet streams are important source regions for the development of low-level cyclones. The acceleration (deceleration) of zonal winds at the entrance (exit) of the jet stream requires ageostrophic meridional flows. These induce vertical circulations on the plane across the jet stream, which connects upper- and low-level circulations (Blackmon *et al.,* 1977). The JJA mean may smooth out the transient activity of the secondary circulations. Nonetheless, considering the modest meandering of the summertime subtropical westerly jet, the generation of the low-level vorticity due to the secondary circulation should be confined near the JJA mean jet streams. In fact, the observed 850-hPa cyclonic vorticity over Korea and Japan is placed around the upper-level jet streak and is generally running parallel with the activity center of the eastward winds. This may be indicative of close connection between the upper- and low-level circulations. Two more local extremes could be also identified: the cyclonic vorticity over Manchuria and the negative vorticity over the northwestern Pacific Ocean. The former is related to the synoptic-scale transient motions, whereas the western Pacific subtropical high (WPSH) is the cause of the latter.

Obviously the CTL fails to capture the positive vorticity around the jet core as well as the negative vorticity over the western North Pacific (Fig. 8b). Further analysis on monthly fields reveals that in July the simulated 200-hPa jet with a maximum strength of about 25 m s^{-1} migrates toward higher latitude (figure not shown), while the observed one yet stays over South Korea and central Japan with an enhanced intensity of about 30 m s^{-1}. Recently Sampe and Xie (2010) showed that the westerly jets anchor the frontal rainband by steering weather disturbances and promote convection through convective instability and adiabatic updrafts.

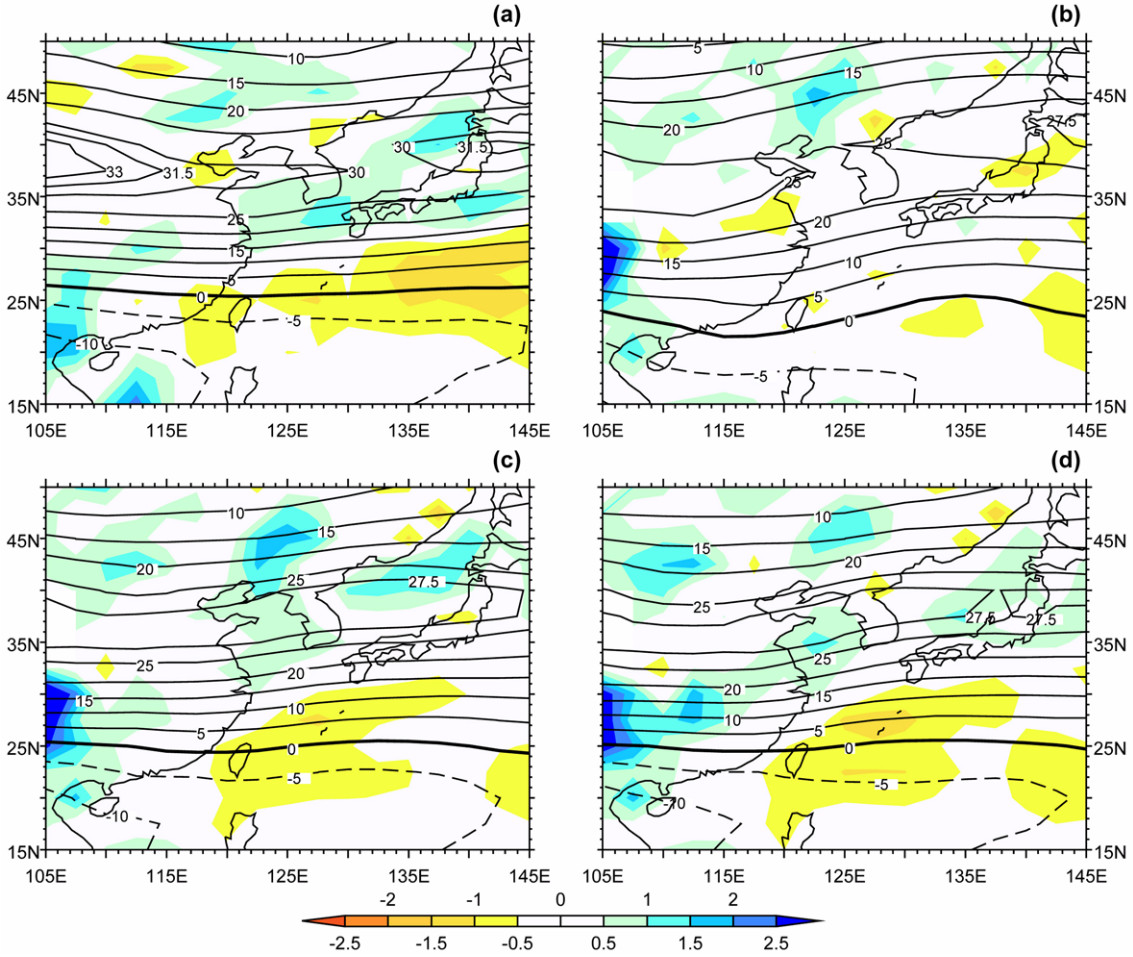

Fig. 8. The JJA mean 200-hPa zonal winds (contours, m s^{-1}) and 850-hPa relative vorticity (shadings, 10^5 s^{-1}) in 1993 for (a) the observation, (b) the CTL, (c) the SWG and (d) SWT. Contour intervals for observation (simulations) are 5 within ± 30 (25) and 1.5 (2.5) outside.

As such, the rapid movement and the weak intensity of the jet would be a primary reason for the poor performance of the 850-hPa vorticity. In contrast, the results of the Goddard scheme in Figs. 8c and 8d display appreciable improvements. The 200-hPa westerly winds tend to become stronger. Furthermore, the northeast-southwest tilt of the monsoon front and the subtropical high over the western north Pacific depicted by the low-level vorticity are reproduced reasonably well.

c. Differential heating and East Asia monsoon

As discussed in section 2b, atmospheric heat source induced by the land-sea thermal contrast can be identified by VIT. Figure 9 shows JJA anomaly of the simulated VIT and 200-hPa wind obtained from the CTL (Fig. 9a), the SWG (Fig. 9b) and the SWT (Fig. 9c). The modeled VIT shows cold anomaly over eastern China in all experiments which is in opposition to the

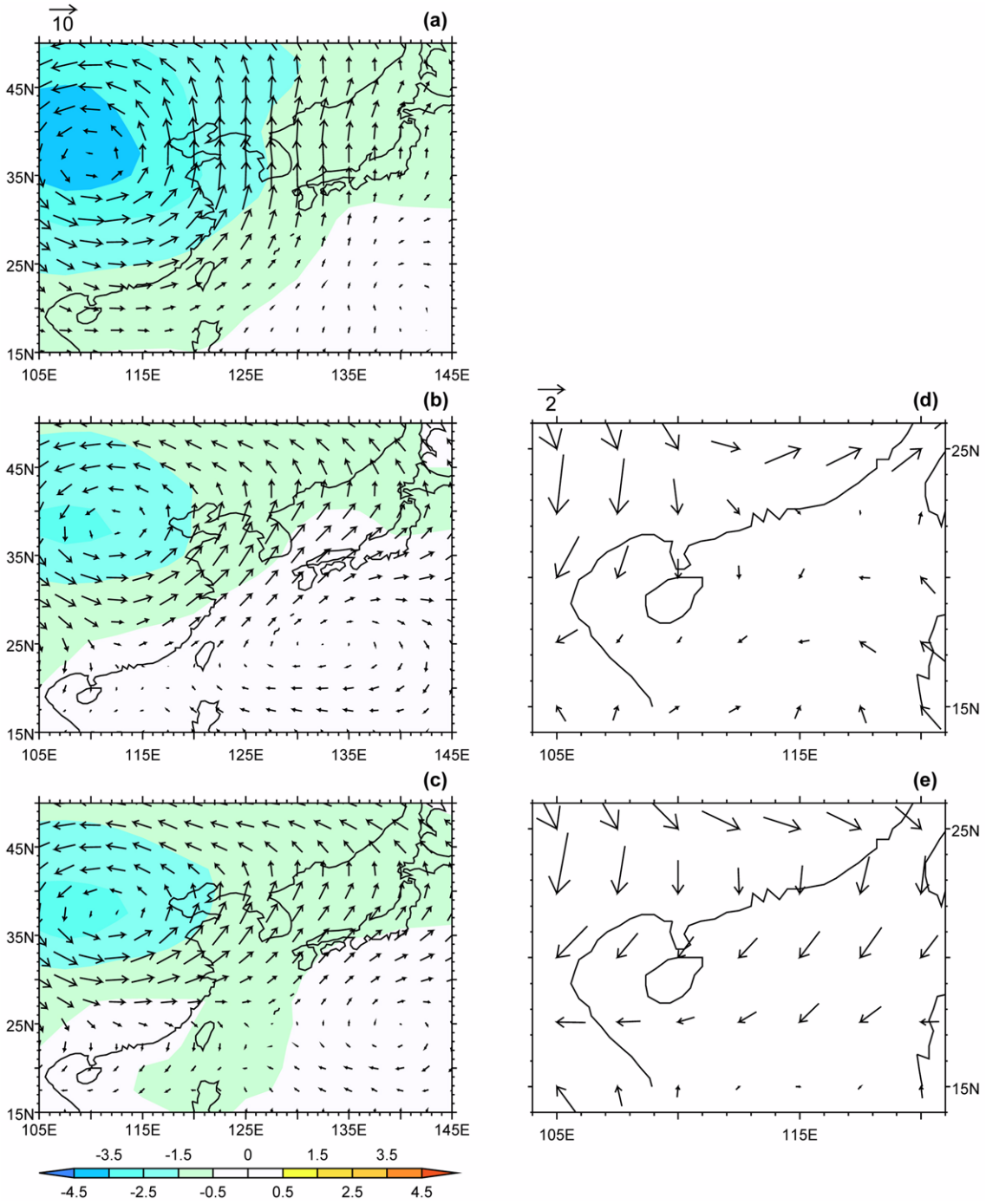

Fig. 9. The simulated JJA anomaly of 200-hPa winds (vectors, m s^{-1}) and VIT (shadings, °C) in 1993 for (a) the CTL, (b) the SWG and (c) the SWT. (d) and (e) are enlargement of (b) and (c) over the area of 105-120°E, 15-25°N, respectively.

observed warm anomaly. However, the simulated 200-hPa wind anomalies differ among the experiments. The CTL simulation, for example, is amiss with the observed features of the northeasterlies over southern China, showing prevailing eastward wind anomalies. Meanwhile, the rest illustrates improved wind anomalies due to the weakening of the cold VIT anomaly. And again, the SWT is in best agreements with observation, reproducing to some degree the enhanced northeasterly over southern China (see Figs. 9d and 9e for close-ups of Figs. 9b and 9c).

The accompanied low-level branch of the monsoon flows also becomes relatively realistic in the SWG and the SWT. In observations, the anomalous northwesterly and southwesterly meet around 30°N over eastern China and coincide with the enhanced rainfall. This convergence zone extends farther to the east (Fig. 10a). In the CTL, in comparison, the anomaly convergence zone reaches far more northward, resulting in unrealistic negative rainfall over central and eastern China, South Korea, and southern Japan where the observation shows normal or above-than-normal precipitation (Fig. 10b). On the other hand, the anomalous low-level winds in the SWG and the SWT converge at below 35°N and the confluent winds extend to the east of Japan (Figs. 10c and 10d). This rectifies the fictitious negative rainfall anomaly over South Korea and southern Japan simulated in the CTL. However, the southwesterly flows over southeastern China and related precipitation are seriously exaggerated regardless of the choice of radiation scheme and top boundary.

d. Quantitative evaluations

In order to quantitatively assess the sensitivity of the WRF model, the Taylor diagram analysis (Taylor 2001) is applied to the seasonal anomaly (Fig. 11). The Taylor diagram is able to provide three statistics such as ratio of the variances, pattern correlation, and centered root-mean-square (RMS) difference between the model-simulated and observed patterns in a concise and easily interpretable manner. Note that all statistics shown in Fig. 11 are area-weighted values.

The correlation coefficient measured by the angle that each symbol makes with abscissa is increased from the CTL (black) to the results with the Goddard scheme (blue for the SWG and red for the SWT). This is especially the case for the temperature fields, such as temperature gradient and VIT, due to the primary impact of shortwave radiation parameterization on a model's thermal structure. The normalized standard deviation gauged by the radial distance from the origin to each symbol also tends to

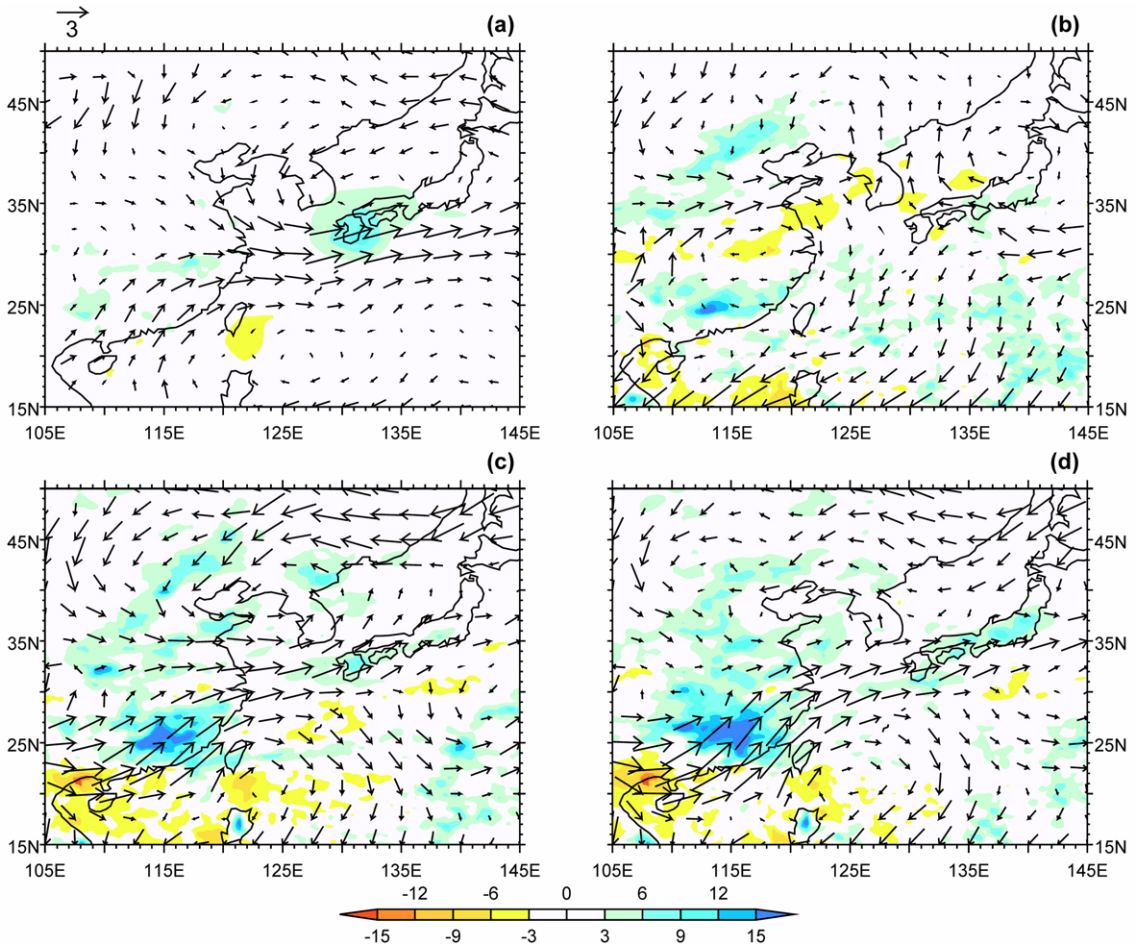

Fig. 10. The simulated JJA anomaly of 850-hPa winds (vectors, m s^{-1}) and precipitation (shadings, mm d^{-1}) in 1993 for (a) the observation, (b) the CTL, (c) the SWG and (d) the SWT.

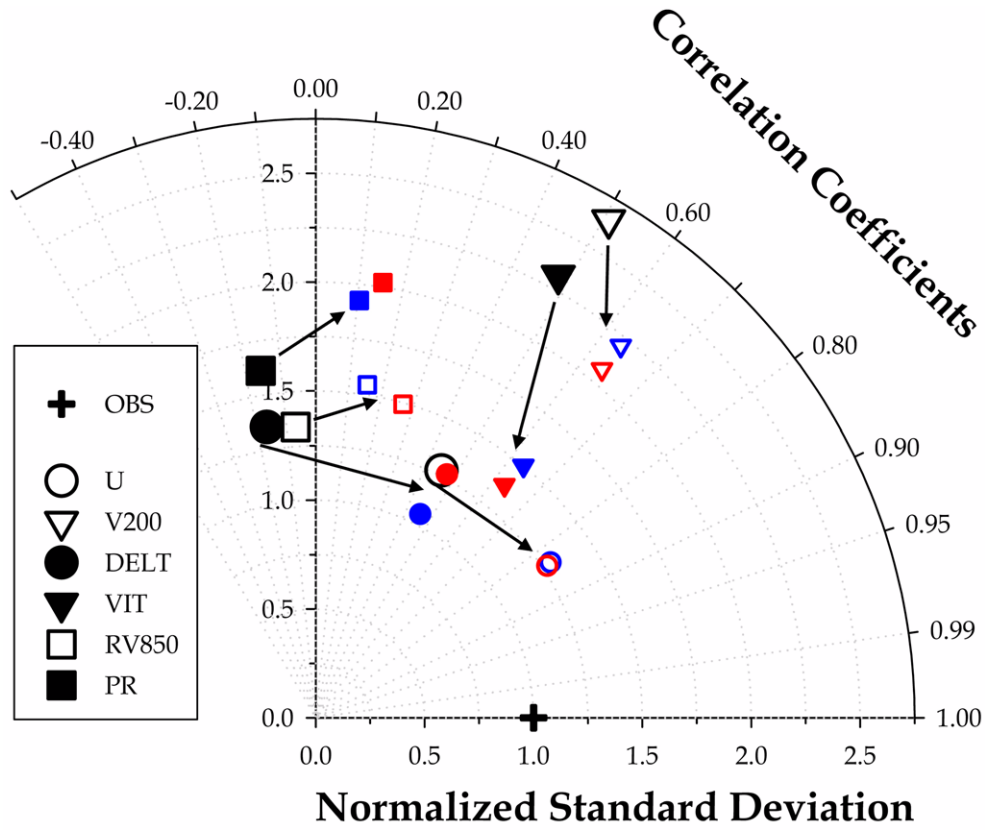

Fig. 11. Taylor diagram for the modeled JJA anomaly obtained from the CTL (black), the SWG (blue) and the SWT (red) experiment. The cross at the unit point on the abscissa indicates observation (U: Latitude-height cross section of zonal winds, V200: Meridional winds at 200 hPa, DELT: Latitudinal temperature gradient, VIT: Vertically integrated temperature, RV850: Relative vorticity at 850 hPa, PR: Precipitation).

approach the observed.

Of particular note is that the SWG and the SWT are distinguishable from each other with the SWT showing slightly improved simulations. The stratospheric thermal structure of the SWT would be influenced additionally by diffusion processes as the elevated top boundary is also favorable for them to occur. However, radiative effects (especially, ozone heating) generally outstrip vertical mixings. Hence it can be said that inclusion of ozone maximum height in association with the extended model top could play a nontrivial role in the EASM simulation.

5. Summary and concluding remarks

Shortwave radiation is one of the fundamental driving forces on seasonal or longer timescale numerical simulation (Kim *et al.,* 2009). In spite of its essential role, very few studies have been devoted to the effects of solar radiation parameterization on RCM simulation. In this context, the authors examined the WRF model's sensitivity in simulating the EASM in 1993 to the different choice of solar radiation parameterizations. Furthermore, it was investigated that to what extent the model simulations are affected by ozone absorption of shortwave radiation. To this end, atmospheric large-scale features obtained from three different numerical experiments were analyzed and compared with the observations with particular focus on the fidelity of the reproduced summertime mean and its climatological anomaly.

The use of the Goddard scheme exerts profound influence on representing the observed seasonal mean and anomaly of zonal mean air temperature and its latitudinal gradient as well as the VIT in the summer of 1993. As a consequence, the SWG and the SWT compare more favorably than the CTL to the observations in modeling the upper- and lower level winds. Besides, the contributing role of ozone attenuation and vertical resolution is unveiled by comparing the SWG and the SWT. A plausible explanation is the means by which the increased vertical layers above 50 hPa leads to a refined and realistic shortwave heating rate in the SWT, which after all results in the improved air temperature. A statistical evaluation confirms the nontrivial role of the advanced radiation scheme and the inclusion of ozone maximum height on the EASM simulation.

However, it should be pointed out that our study uses the Betts-Miller-Janjić and the Lin schemes for convective and non-convective rain processes, even though there are many other parameterizations in the WRF model. The different combination of the precipitation schemes may result in different precipitation patterns, which affects the atmospheric temperature through latent heat release. In addition, the choice of an abnormal case could undermine the generality of the present study. Therefore further sensitivity tests to precipitation parameterizations and weather conditions (*e.g.*, dry and/or normal years) are needed to

assure the results discussed here.

Despite of such limitations, the importance of inclusion of ozone maximum height has a considerable implication. Yu *et al*. (2004) showed observational evidences for the relationship between the lower stratospheric temperature change and upper tropospheric cooling trend over East Asia during July and August. Xin *et al*. (2006) further suggested that the upper-tropospheric cooling induces an anomalous meridional cell with descending (ascending) motion occurring beneath (to the south of) the cooling region, which explains the decadal change of the precipitation over South China. These features appear to be reproducible in a numerical model (Xin *et al.,* 2008). Furthermore, the Tibetan Plateau -the origin of the elevated heat source for the Asian monsoon- is known as an active region of troposphere-stratosphere interaction due to extremely active deep convection during summer. As a result, ozone depletion was found to be significant (Tobo *et al.,* 2008). The impact of ozone variation and its radiative effects on EASM, however, has been overlooked for decades. Therefore careful treatment for the ozone solar heating conducted in this study could be used as an effective methodology to fill such gap.

Acknowledgments. We thank the anonymous reviewers for valuable and insightful comments which significantly help to improve the manuscript. This study was supported by Ministry of Environment of Korea as "The Eco-technopia 21 project". B. Wang also acknowledges support from the Korea Meteorological Administration Research and Development Program under Grant RACS 2010-2017.

REFERENCES

Adler, R. F., and Coauthors, , 2003: The Version 2 Global Precipitation Climatology Project (GPCP) monthly precipitation analysis (1979-present). *J. Hydrometeorol*., **4**, 1147-1167.

Blackmon, M. L., J. M. Wallace, N.-C. Lau, and S. L. Mullen, 1977: An observational study of the Northern Hemisphere wintertime circulation. *J. Atmos. Sci*., **34**, 1040-1053.

Chen, F., and J. Dudhia, 2001: Coupling an advanced land-surface/hydrology model with the Penn State/NCAR MM5 modeling system. Part I: Model description and implementation. *Mon. Wea. Rev*., **129**, 569-585.

Chou, M.-D., and M. J. Suarez, 1999: A shortwave radiation parameterization for atmospheric studies. NASA Tech. Memo., **15(104606)**, 40 pp.

Davis, C. A., K. W. Manning, R. E. Carbone, S. B. Trier, and J. D. Tuttle, 2003: Coherence of warm season continental rainfall in numerical weather prediction model. *Mon. Wea. Rev*., **131**, 2667-2679.

Ding, Y.-H., 1992: Summer monsoon rainfall in China. *J. Meteor. Soc. Japan*., **70(1B)**, 373-396.

Dudhia, J., 1989: Numerical study of convection observed during the winter monsoon experiment using a mesoscale two-dimensional model. *J. Atmos. Sci*., **46**, 3077-3107.

Dyer, A. J., and B. B. Hicks, 1970: Flux-gradient relationships in the constant flux layer. *Quart. J. Roy. Meteor. Soc.*, **96**, 715-721.

Fortuin, A. P. F., and H. Kelder, 1998: An ozone climatology based on ozonesonde and satellite measurements. *J. Geophys. Res*., **103**, 31, 706-31, 734.

Fu, Q., and K. N. Liou, 1992: On the correlated k-distribution method for the radiative transfer in nonhomogeneous atmospheres. *J. Atmos. Sci*., **49**, 2139-2156.

Giorgi, F, and L. O. Mearns, 1999: Introduction to special section: Regional climate modeling revisited. *J. Geophys. Res*., **104**, 6335–6352.

Goswami, B. N., and P. K. Xavier, 2005: ENSO control on the south Asian monsoon through the length of the rainy season. *Geophys. Res. Lett*., **32**, L18717, doi:10.1029/2005GL023216.

He, H., C.-H. Sui, M. J. Jian, Z. Wen, and G. Lan, 2003: The evolution of tropical temperature field and its relationship with onset of Asian summer monsoon. *J. Meteor. Soc. Japan*., **81**, 1201-1223.

Hong, S.-Y., Y. Noh, and J. Dudhia, 2006: A new vertical diffusion package with an explicit treatment of entrainment processes. *Mon. Wea. Rev*., **134**, 2318-2341.

Iacono, M. J., E. J. Mlawer, S. A. Clough, and J.-J. Morcrette, 2000: Impact of an improved longwave radiation model, RRTM, on the energy budget and thermodynamic properties of the NCAR community climate model, CCM3. *J. Geophys. Res*., **105(D11)**, 14, 873-14, 890, doi:10.1029/2000JD900091.

Janjić, Z. I., 1994: The step-mountain Eta coordinate model: Further developments of the convection, viscous sublayer, and turbulence closure schemes. *Mon. Wea. Rev*., **122**, 927-945.

Kanamitsu, M., W. Ebisuzaki, J. Woollen, S.-K. Yang, J. J. Hnilo, M. Fiorino, and G. L. Potter, 2002: NCEP-DOE AMIP-II Reanalysis (R-2). *Bull. Amer. Meteor. Soc*., **83**, 1631-1643.

Kang, H.-S., D.-H. Cha, and D.-K. Lee, 2005: Evaluation of the mesoscale model/land model (MM5/LSM) coupled model for East Asian summer monsoon simulations. *J. Geophys. Res*., **110**, D10105, doi:10.1029/2004JD005266.

Kawamura, R., and T. Murakami, 1998: Baiu near Japan and its relation to summer monsoons over Southeast Asia and the western North Pacific. *J. Meteorol. Soc. Jpn*., **76**, 619-639.

Kim, H.-J., I.-U. Chung, and K.-T. Lee, 2009: Effects of an advanced radiation parameterization on a troposphere-stratosphere AGCM simulation. *Asia-Pacific J. Atmos. Sci*., **45**, 439-462.

Knievel, J. C., D. A. Ahijevych, and K. W. Manning, 2004: Using temporal modes of rainfall to evaluate the performance of a weather prediction model. *Mon. Wea. Rev*., **132**, 2995-3009.

Lee, D.-K., and M.-S. Suh, 2000: Ten-year East Asian summer monsoon simulation using a regional climate model (RegCM2). *J. Geophys. Res*., **105**, 29,565-29,577.

_____, H.-S. Kang, and K.-H. Min, 2002: The role of ocean roughness in regional climate modeling: 1994 East Asia summer monsoon case. *J. Meteor. Soc. Japan*., **80**, 171-189.

_____, D.-H. Cha, and H.-S. Kang, 2004: Regional climate simulation of the 1998 summer flood over East Asia. *J. Meteor. Soc. Japan*., 82, 1735-1753.

Lin, Y-L, R. D. Farley, and H. D. Orville, 1983: Bulk parameterization of the snow field in a cloud model. *J. Climate. Appl. Meteor*., **22**, 1065-1092.

Liou, K. N., 2002: An Introduction to Atmospheric Radiation., Elsevier., 583pp

Lo, J. C.-F., Z.-L. Yang, and R. A. Pielke Sr., 2008: Assessment of three dynamical climate downscaling methods using the Weather Research and Forecasting (WRF) model. *J. Geophys. Res*., **113**, D09112, doi:10.1029/2007JD009216.

Mlawer, E. J., S. J. Taubman, P. D. Brown, M. J. Iacono, and S. A. Clough, 1997: Radiative transfer for inhomogeneous atmospheres: RRTM, a validated correlated-k model for the longwave. *J. Geophys. Res*., **102(D14)**, 16, 663-16, 682, doi:10.1029/97JD00237.

Park, C.-K., and S. D. Schubert, 1997: On the nature of the 1994 East Asian summer drought. *J. Climate*, **10**, 1056-1070.

Paulson, C. A., 1970: The mathematical representation of wind speed and temperature profi les in the unstable atmospheric surface layer. *J. Appl. Meteor.*, **9**, 857-861.

Salathé, E. P., L. R. Leung, Y. Qian, and Y. Zhang, 2010: Regional climate model projections for the State of Washington. *Climatic Change*, **102**, 51-75.

Sampe, T. and S.-P. Xie, 2010: Large-scale dynamics of the Meiyu-Baiu rain band: Environmental forcing by the westerly jet. *J. Climate*, **23**, 113-134.

Skamarock, W. C., J. B. Klemp, J. Dudhia, D. O. Gill, D. M. Barker, W. Wang, and J. G. Powers, 2005: A Description of the Advanced Research WRF Version 2. NCAR/TN-468+STR, 88 pp.

Taylor, K. E., 2001: Summarizing multiple aspects of model performance in a single diagram. *J. Geophys. Res*., **106**, 7183-7192.

Tobo, Y., Y. Iwasaka, D. Zhang, G. Shi, Y.-S. Kim, K. Tamura, and T. Ohashi, 2008: Summertime "ozone valley" over the Tibetan Plateau derived from ozonesondes and EP/TOMS data. *Geophys. Res. Lett*., **35**, L16801, doi:10.1029/2008GL034341.

Ueda, H. and T. Yasunari, 1998: The role of warming over the Tibetan Plateau in early onset of the summer monsoon over the Bay of Bengal and the South China Sea. *J. Meteor. Soc. Japan*., **76**, 1-12.

Uppala, S. M., P. W. Kallberg, A. J. Simmons, U. Andrae, V. da Costa Bechtold, M. Fiorino, J. K. Gibson, J. Haseler, A. Hernandez, G. A. Kelly, and X. Li, 2005: The ERA-40 Reanalysis. *Quart. J. Roy. Meteor. Soc*., **131**, 2961-3012.

Wang, W.-C., W. Gong, and H. Wei, 2000: A regional model simulation of the 1991 severe precipitation event over the Yangtze-Huai river valley. Part I: Precipitation and circulation statistics. *J. Climate*, **13**, 74-92.

Webb, E. K., 1970: Profile relationships: The log-linear range, and extension to strong stability. *Quart. J. Roy. Meteor. Soc.*, **96**, 67-90.

Wicker, L. J., and W. C. Skamarock, 2002: Time-splitting methods for elastic models using forward time schemes. *Mon. Wea. Rev*., **130**, 2088-2097.

Xin, X., R. Yu, T, Zhou, and B. Wang, 2006: Drought in late spring of South China in recent decades. *J. Climate*, **19**, 3197-3206.

_____, Z. Li, R. Yu, and T. Zhou, 2008: Impacts of upper tropospheric cooling upon the late spring drought in East Asia simulated by a regional climate Model. *Adv. Atmos. Sci*., **25**, 555-562.

Yoo, S.-H., C.-H. Ho, S. Yang, H.-J. Choi, and J.-G. Jhun, 2004: Influence of tropical western and extratropical Pacific SST on East and Southeast Asia climate in the summer of 1993-94. *J. Climate*, **17**, 2673-2687.

Yu, R., B. Wang, and T. Zhou, 2004: Tropospheric cooling and summer monsoon weakening trend over East Asia. *Geophys. Res. Lett*., **31**, L22212, doi:10.1029/2004GL021270.

Zhang, Y., X. Kuang, W. Guo, and T. Zhou, 2006: Seasonal evolution of the upper-tropospheric westerly jet core over East Asia. *Geophys. Res. Lett*., **33**, L11708, doi:10.1029/2006GL026377.

Zhou, T.-J., and R.-C. Yu, 2005: Atmospheric water vapor transport associated with typical anomalous summer rainfall patterns in China. *J. Geophys. Res*., **110**, D08104, doi:10.1029/2004JD005413.